Journal of Membrane Science 643 (2022) 120064

Contents lists available at ScienceDirect

Journal of Membrane Science

journal homepage: www.elsevier.com/locate/memsci

Fabrication of MIL-96 nanosheets and relevant *c*-oriented ultrathin membrane through solvent optimization

Sixing Chen [a], Yi Liu [a], Yanwei Sun [a], Guoliang Xu [a], Taotao Ji [a], Xiongfu Zhang [a,b], Fei Wang [c], Yi Liu [a,b,*]

[a] State Key Laboratory of Fine Chemicals, School of Chemical Engineering, Dalian University of Technology, Linggong Road 2, Ganjingzi District, Dalian, 116024, China
[b] Dalian Key Laboratory of Membrane Materials and Membrane Processes, Dalian University of Technology, Linggong Road 2, Ganjingzi District, Dalian, 116024, China
[c] State Key Laboratory of Structural Chemistry, Fujian Institute of Research on the Structure of Matter, Chinese Academy of Sciences, Fuzhou, 350002, China

ARTICLE INFO

Keywords:
Metal-organic framework
Nanosheets
Orientation
Secondary growth
Gas separation

ABSTRACT

Concurrent manipulation of orientation and thickness of MOF membranes has become a reliable approach for improving their separation performances. In terms of oriented seeded growth, oriented deposition of MOF nanosheets during seeding process and sealing all intergranular gaps with no discernible increase in membrane thickness during secondary growth have become indispensable. In this study, we pioneered the fabrication of uniform hexagonal-shaped, 20–40 nm thick MIL-96 nanosheets through solvent composition optimization ($V_{H2O}/V_{FA} = 1/2$). Subsequently, spin coating was employed for *c*-oriented deposition of uniform MIL-96 seed layer, during which the addition of PVP in the suspension was found to be critical for obtaining qualified seed layer. Finally, well-intergrown, highly *c*-oriented ultrathin MIL-96 membrane was prepared upon employing NMF as the solvent during secondary growth. Gas permeation results implied that prepared MIL-96 membrane exhibited superior gas separation performance compared with that of *a*-&*b*-oriented counterpart.

1. Introduction

In recent decades, fabrication of highly oriented ultrathin MOF membranes has become a reliable approach for improving their separation performances due to highly ordered pore arrangement and reduced gas diffusion path length [1–9]. Lai et al. pioneered the fabrication of dense and continuous (102)-oriented MOF-5 membranes through oriented seeded growth [10]. Through controlled epitaxial growth of randomly oriented seed layers, Caro et al. prepared preferentially *c*-oriented ZIF-7 membrane and (100)-oriented ZIF-8 membrane exhibiting superior H_2/N_2 and H_2/C_3H_8 selectivity, respectively [11,12]. Huang et al. prepared highly *c*-oriented ZIF-95 membrane with superior H_2/CH_4 separation performance through vapor-assisted in-plane epitaxial growth of the oriented ZIF-95 seed layer [13]. We recently reported the fabrication of highly *c*-oriented NH_2-MIL-125 membrane with superior H_2/CO_2 selectivity through combining dynamically oriented seeding and single-mode microwave heating-assisted in-plane epitaxial growth [14]. In the same manner, highly (111)-oriented NH_2-UiO-66 membrane exhibiting superior H_2/CO_2 separation permeance was prepared with ZrS_2 as zirconium source during epitaxial growth [15]. Nevertheless, it remained a great challenge in terms of oriented ultrathin 3D MOF membrane preparation due to the difficulty in preparation of ultrathin MOF nanosheet (NS) seeds, oriented deposition of qualified seed layer, and effective patching of intergranular gaps with no discernible increase in membrane thickness during secondary growth [16–22].

MIL-96 (Al), a porous aluminum trimesate 3D MOF material composed of aluminium clusters [$Al_3(\mu_3\text{-}O)$ $(BTC)_6$] and infinite chains of $AlO_4(OH)_2$ and $AlO_2(OH)_4$ octahedra [23–28], has shown great promise in catalysis [29], sensing [30], gas adsorption/separation [28,31], and water purification [32]. Simultaneously, MIL-96(Al) was considered as a promising membrane material due to its high CO_2 adsorption capacity and excellent hydrothermal stability [33]. Caro et al. prepared *a*-&*b*-oriented MIL-96 membrane showing decent H_2/CO_2 selectivity [34]. Further analysis on the pore structure of MIL-96 crystals in different directions implied that MIL-96 membrane exhibiting *c*-axis preferred orientation should be more conducive to the separation of H_2 from other gas molecules since the pore size along the *c*-axis was

* Corresponding author. State Key Laboratory of Fine Chemicals, School of Chemical Engineering, Dalian University of Technology, Linggong Road 2, Ganjingzi District, Dalian, 116024, China.
E-mail address: diligenliu@dlut.edu.cn (Y. Liu).

https://doi.org/10.1016/j.memsci.2021.120064
Received 14 September 2021; Received in revised form 6 November 2021; Accepted 9 November 2021
Available online 16 November 2021

the smallest (Fig. S1). In this study, we pioneered the fabrication of well-intergrown, highly *c*-oriented ultrathin MIL-96 membrane via oriented seeded growth (shown in Fig. 1). Our study indicated that among various synthetic factors, the fabrication of uniform MIL-96 NS seeds, the addition of trace amount of PVP in the seed suspension for spin coating, and the use of NMF as solvent during secondary growth played vital roles in the preparation of MIL-96 membrane with desired microstructure. Gas permeation results indicated that both H_2 permeance and H_2/CO_2 selectivity of prepared MIL-96 membrane was much higher than that of *a*-&*b*-oriented counterpart, thereby confirming the significance of concurrent orientation and thickness control in separation performance enhancement of relevant MOF membranes.

2. Experimental section

2.1. Chemicals

Aluminum nitrate nonahydrate ($Al(NO_3)_3{\cdot}9H_2O$, 98%) and 1,3,5-benzenetricarboxylic (H_3BTC, 98%) were purchased from ALADDIN Reagent, Shanghai; N, *N*-dimethylformamide (DMF, 99.8%) and acetic acid (HAc, 99.8%) were purchased from Kermel, Tianjin; *N*-methylformamide (NMF, 99%), formamide (FA, 99%) and polyvinylpyrrolidone (PVP, average M_W: ~58000) were purchased from Macklin, Shanghai; porous α-Al_2O_3 ceramic discs with ~70 nm pore size were purchased from Fraunhofer IKTS (Germany).

2.2. Preparation of MIL-96 crystals with varying morphology

MIL-96 NSs were prepared as follows: Initially, 1.26 g $Al(NO_3)_3{\cdot}9H_2O$ was dissolved in 8 mL deionized water, and 0.63 g H_3BTC was dissolved in 16 mL FA, respectively. Subsequently, the above clear solutions were mixed in an 80 °C ultrasonic bath for 15 min, during which 1 mL of 10 mM HAc was added. In the next step, the above solution was poured in a Teflon-lined autoclave and placed in an oven preheated to 210 °C. After an elapse of 2 h, the autoclave was taken out from the oven. Solid products were obtained by repeated centrifugation and washing with water and methanol three times, respectively.

MIL-96 powders with other morphologies were prepared with 8 mL DMF, 8 mL NMF and 8 mL FA as solvents instead of 16 mL FA while keeping other reaction conditions unchanged.

2.3. Preparation of c-oriented MIL-96 seed layer

The MIL-96 seed suspension was prepared by adding 125 mg MIL-96 powders in 5 mL methanol. Subsequently, 10 μL of 0.01 mM PVP aqueous solution was added in the above suspension and vigorously stirred for 24 h before use. In the next step, 0.1 mL seed suspension was dropped onto the α-Al_2O_3 plate surface, and then spin coating was conducted at 3000 rpm for 60 s. Finally, obtained seed layer was dried at 70 °C overnight.

2.4. Preparation of c-oriented ultrathin MIL-96 membrane

1.26 g $Al(NO_3)_3{\cdot}9H_2O$ was dissolved in 8 mL deionized water, and 0.63 g H_3BTC was dissolved in 16 mL NMF, respectively. Subsequently, the above solutions were mixed in an 80 °C ultrasonic bath for 15 min, during which 1 mL of 10 mM HAc was added. In the next step, the precursor solution was poured into a 50 mL Teflon-lined autoclave in which the MIL-96 NS seed layer-modified α-Al_2O_3 substrate was vertically placed. Solvothermal reaction was conducted at 210 °C for 2 h. After cooling to room temperature, the membrane was taken out, thoroughly washed with methanol, and finally dried at 70 °C overnight.

2.5. Preparation of a-&b-oriented MIL-96 membrane

As a comparative experiment, *a*-&*b*-oriented MIL-96 membrane was prepared with 16 mL FA as solvent instead of 16 mL NMF while keeping other reaction conditions unchanged.

2.6. Characterization

Morphology of prepared samples was measured by SEM (Hitachi FlexSEM 1000), TEM (JEOL JEM 2100) and AFM (MI PicoScan 2500). XRD patterns were measured on a Rigaku SmartLab diffractometer with Cu Kα radiation (λ = 0.15418 nm).

2.7. Gas permeation test

Prepared MIL-96 membrane was fixed in a module sealed with silicone O-rings, and the permeation properties were evaluated by both single gas permeation and mixed gas separation. Ar (50 mL min^{-1}) was used as sweep gas. In mixed gas permeation measurement, 1:1 binary gas mixture was applied to the feed side of the MIL-96 membrane, and

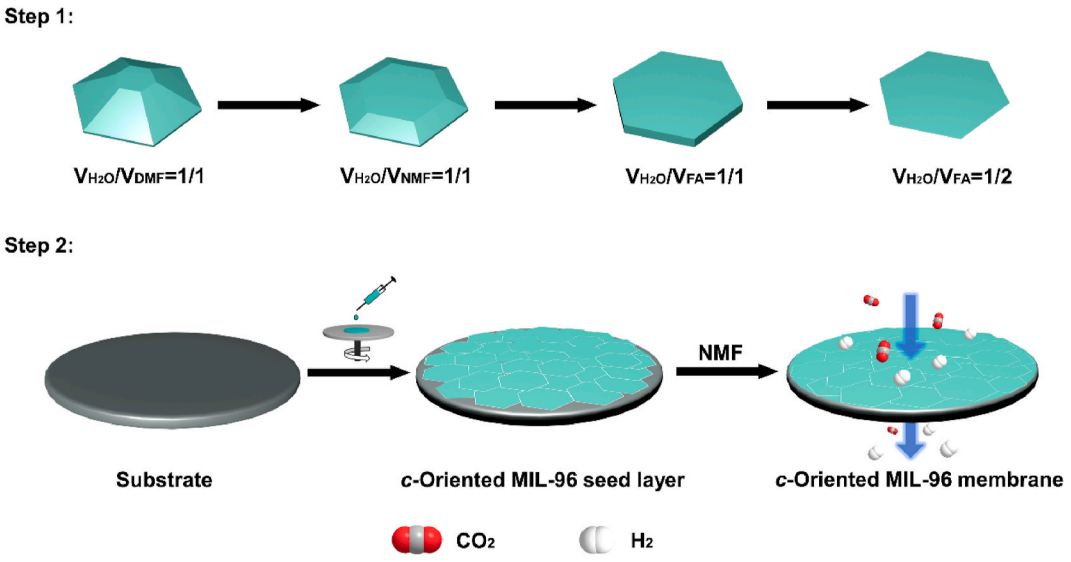

Fig. 1. Schematic illustration of the preparation of MIL-96 membrane. Step 1 illustrated the preparation of hexagonal-shaped ultrathin MIL-96 nanosheets through solvent optimization. Step 2 illustrated the preparation of highly c-oriented ultrathin MIL-96 membrane preparation via oriented seeded growth.

the permeate gas was removed from the permeate side by sweep gas. Both flow rates of the feed side and the sweep side were set to 50 mL min^{-1} and the pressure difference was kept at 1 bar. In single gas permeation measurement, the flow rates were set to 50 mL min^{-1}, the permeate gas was removed from the permeate side by sweep gas, and the pressure difference on two sides was kept at 1 bar. The concentration of mixed gases in the permeate side was detected by using a gas chromatograph (GC7900, Tencomp). The permeance (P) was described by division of the flux by the transmembrane pressure difference, as shown in Eq. (1), where n was the amount of gas in mol, A was the membrane area, t was the permeation time, and Δp was the pressure difference. The ideal selectivity α_{ideal} was defined as the ratio of the single component permeance (i, j) as shown in Eq (2). The separation factor (SF) $\alpha_{i/j}$ for the permeation of binary gas mixture was described as the quotient of the molar ratio of the permeate side components (i, j) divided by that of the feed side components (i, j) as shown in Eq. (3).

$$P = \frac{n}{A \times t \times \Delta p} \tag{1}$$

$$\alpha_{ideal} = \frac{P_{i,single}}{P_{j,single}} \tag{2}$$

$$\alpha_{i/j} = \frac{X_{i,perm} / X_{j,perm}}{X_{i,feed} / X_{j,feed}} \tag{3}$$

3. Results and discussion

3.1. Preparation of MIL-96 NSs

The first step involved preparation of ultrathin MIL-96 NSs. At present, several methods, including the use of dual Al sources, the introduction of competitive ligands, and the addition of surfactants/alkaline modulators, have been developed to regulate the morphology of MIL-96 powders [35–38]. Nonetheless, a reliable method for preparation of ultrathin NS seeds, which was indispensable for the fabrication of ultrathin MIL-96 membrane, remained unexplored to date. Herein we attempted to solve this issue by optimizing the solvent composition. As shown in Fig. 2a, the use of DMF solvent led to the formation of MIL-96 crystals exhibiting a truncated hexagonal bipyramidal morphology; nevertheless, a large thickness in the c-axis direction (1.7 μm) as well as relatively low aspect ratio (ca. 1.4) made them unsuitable for use as seeds. Alternatively, NMF and FA were further used as solvents. It was observed that the morphology of MIL-96 crystals gradually evolved from truncated hexagonal bipyramidal to hexagonal prismatic shape (Fig. 2b and c). In particular, using FA as solvent led to the formation of MIL-96 crystals with remarkably reduced thickness along the c-axis (150 nm) and considerably higher aspect ratio (ca. 4.7). The discrepancy in morphology may be attributed to different hydrolysis rates of the above amide solvents (FA > NMF > DMF) [39,40], resulting in different generation rates of dimethylamine (DMA) and formic acid. Because of its strong basicity, a higher DMA concentration increased the deprotonation rate of H_3BTC ligands, resulting in a higher nucleation rate in the bulk solution and therefore, reduced crystal size; while formic acid, which commonly served as a modulator, may preferentially adsorb on

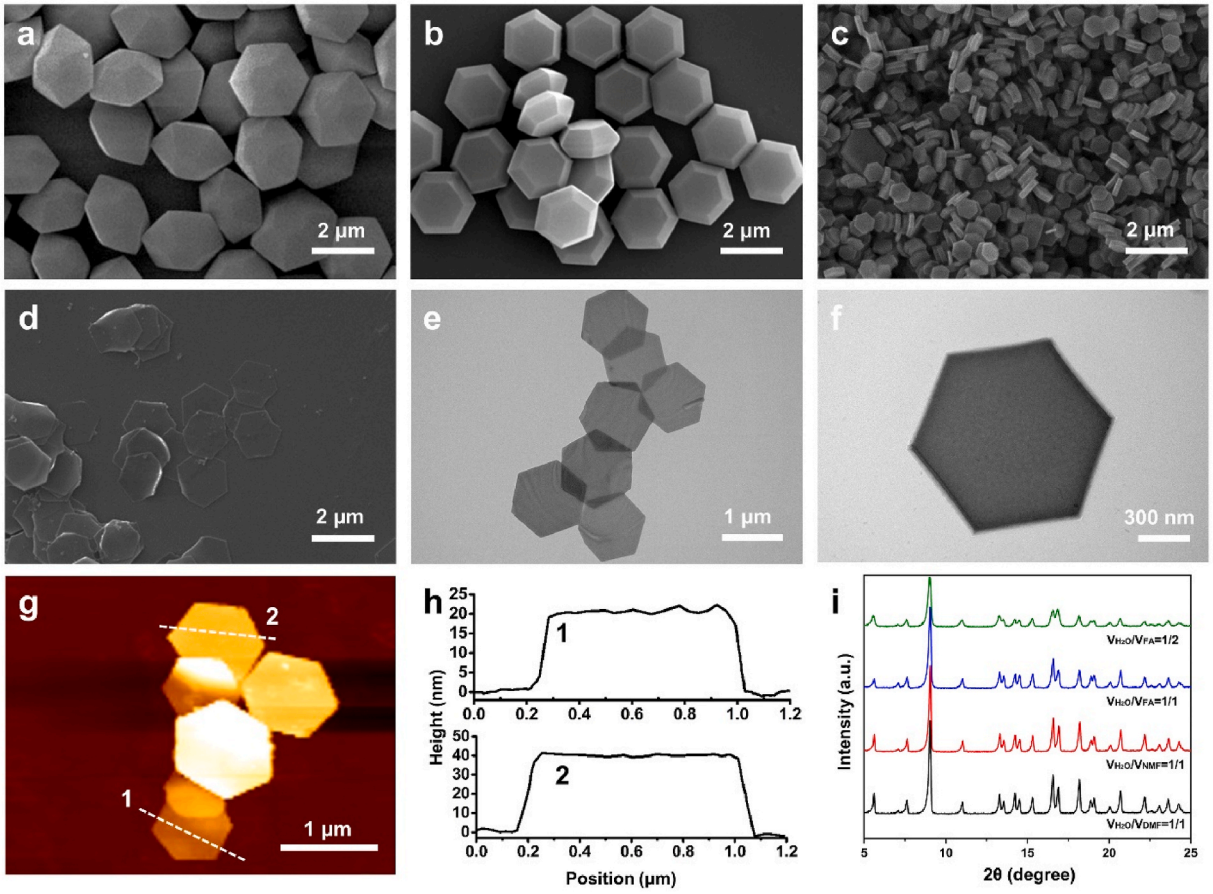

Fig. 2. SEM images of MIL-96 crystals prepared with different solvent composition. (a) $V_{H2O}/V_{DMF} = 1/1$; (b) $V_{H2O}/V_{NMF} = 1/1$; (c) $V_{H2O}/V_{FA} = 1/1$; and (d) $V_{H2O}/V_{FA} = 1/2$. (e, f) TEM images of MIL-96 NSs. (g, h) AFM height image with a height profile along the indicated trace. (i) XRD patterns of MIL-96 crystals prepared with different solvent composition.

the {00*l*} facet and regulate its growth to form hexagonal prismatic MIL-96 crystals with higher aspect ratio [41].

In the next step, FA/H_2O volume ratio (V_{FA}/V_{H2O}) of the precursor solution was tuned to further optimize the morphology of MIL-96 crystals [37]. SEM and TEM images (Fig. 2d–f) showed that in the case that the value of V_{FA}/V_{H2O} increased to 2, uniform hexagonal-shaped MIL-96 NSs could be readily prepared. AFM height image (Fig. 2g and h) indicated that the average thickness of MIL-96 NSs was 20–40 nm along the *c*-axis with much higher aspect ratio (36.5–73.0). To the best of our knowledge, this represented the thinnest MIL-96 NSs ever prepared to date. Corresponding XRD results (Figs. 2i and 3a) confirmed that prepared NSs indeed belonged to pure MIL-96 phase. The superior morphology of MIL-96 NSs obtained made them suitable for use as seeds.

3.2. Oriented deposition of MIL-96 seed layer

Subsequently, spin coating technique was employed to evenly spread ultrathin MIL-96 NS seeds on porous α-Al_2O_3 substrate (Fig. S2). SEM results indicated that the seed layer obtained under optimized conditions was uniform and ca. 170 nm thick (shown in Fig. 4a and b). Relevant XRD pattern (shown in Fig. 3b) further showed that only two conspicuous diffraction peaks located at 2θ values of 5.6° and 17.0°, which corresponded to (002) and (006) crystal planes, appeared, thereby confirming that prepared MIL-96 seed layer was highly *c*-oriented. It is worth noting that addition of PVP in the seed suspension prior to spin coating was indispensable to obtain the seed layer with desired morphology [15]; or else, severe aggregation and curling of MIL-96 seeds would inevitably occur, resulting in the formation of seed layers with uneven seed distribution and excessive intergranular voids (shown in Fig. S3). This can be ascribed to preferential adsorption of PVP molecules to the surface of MIL-96 NSs, which significantly increased their repulsion interactions for better monodispersity in the suspension. As a result, uniform *c*-oriented ultrathin MIL-96 seed layer could be successfully obtained.

3.3. Preparation of c-oriented ultrathin MIL-96 membrane

It is of vital importance to concurrently seal all intergranular gaps, avoid excessive epitaxial growth in the *c*-axis direction, and suppress twin growth of the MIL-96 seed layer during membrane processing. Nevertheless, our study indicated that using FA as solvent inevitably led to severe twinning. As shown in Fig. 4c and d, after secondary growth, the MIL-96 membrane surface had been fully covered with vertically aligned MIL-96 NSs, which could be ascribed to the formation of excessive MIL-96 nuclei in bulk solution and their subsequent sedimentation on the membrane surface, resulting in preferential arrangement of newly formed MIL-96 NSs with their largest faces perpendicular to the substrate (shown in Fig. S4) following the "evolution selection" growth mechanism developed by van der Drift [42]. Relevant XRD pattern further confirmed that prepared MIL-96 membrane was preferentially *a*-&*b*-oriented (shown in Fig. 3c).

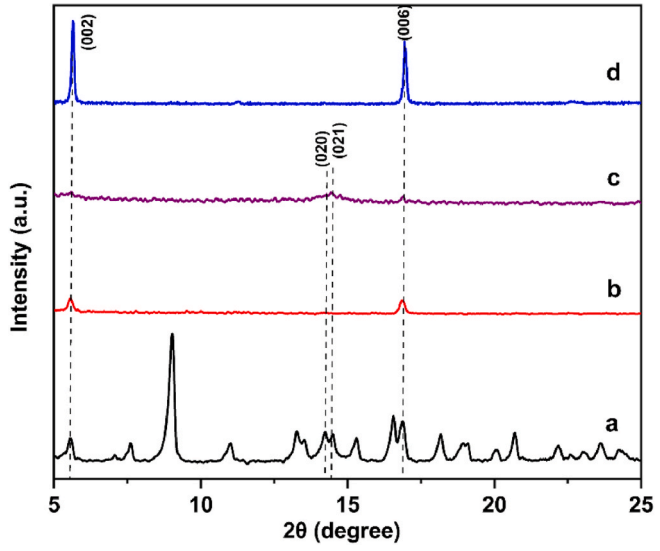

Fig. 3. XRD patterns of a) MIL-96 NSs; b) *c*-oriented MIL-96 seed layer; c) *a*-&*b*-oriented MIL-96 membrane and d) *c*-oriented ultrathin MIL-96 membrane.

Fortunately, undesired twin growth could be effective suppressed by using NMF instead of FA as solvent. SEM results (shown in Fig. 4e and f) showed that after secondary growth under optimized conditions, a well-intergrown 230 nm-thick MIL-96 membrane was obtained. Corresponding XRD pattern (shown in Fig. 3d) showed that prepared membrane remained dominantly *c*-oriented. Moreover, the prepared *c*-oriented ultrathin MIL-96 membrane was ultrasonically treated for 30 min to verify the mechanical stability. Relevant SEM image (Fig. S5a) indicated that not only the surface morphology of ultrasonically treated MIL-96 membrane remained intact but also the XRD pattern (Fig. S5b) was unchanged, implying that strong interaction existed between the membrane and the substrate. The reason for effective twin suppression can be attributed to a relatively poor solubility of BTC ligands in NMF solvent (33 mg/mL at 20 °C) in comparison with FA solvent (46 mg/ml at 20 °C), resulting in effective suppression of nucleation of MIL-96 crystals in the bulk solution so that only epitaxial growth along the crystallographic orientation inherited from the seed layer was maintained during secondary growth. In addition to twin suppression, the use of NMF solvent also significantly promoted the growth rate in the lateral direction. According to calculation, the relative lateral epitaxial growth rate (defined as the ratio of lateral increasing length to vertical increasing length of membrane ($v_{lateral}/v_{vertical}$)) of the seed layer during secondary growth reached 31.2 (Table S1), which was comparable with the aspect ratio of ultrathin MIL-96 NS seeds. As a result, the increase of MIL-96 seed layer thickness in the direction of *c*-axis orientation after secondary growth was negligible.

3.4. Gas permeation properties of prepared MIL-96 membranes

Finally, gas permeation properties of both *c*-oriented ultrathin and *a*-&*b*-oriented MIL-96 membranes were investigated. Our results indicated that ideal H_2/CO_2, H_2/N_2 and H_2/CH_4 selectivity of prepared *a*-&*b*-oriented MIL-96 membrane reached 6.6, 5.9 and 4.9, respectively, which was close to the values reported by Caro et al. (shown in Fig. 5a and b) [34]. In contrast, the ideal H_2/CO_2 selectivity of *c*-oriented ultrathin MIL-96 membrane reached 16.9, which was almost 2.6 times higher than that of *a*-&*b*-oriented counterpart (shown in Fig. 5c and d). Moreover, the H_2 permeance (4.4×10^{-7} mol $m^{-2}s^{-1}Pa^{-1}$) of the former MIL-96 membrane was considerably increased (shown in Table S2), leading to well exceedance of the 2008 Robeson upper bound of polymer membranes for H_2/CO_2 separation (shown in Fig. S6). The superior H_2/CO_2 separation performance of prepared *c*-oriented ultrathin MIL-96 membrane can be ascribed to 1) smaller channels along the *c*-axis, which is more suitable for accurate screening of H_2 and CO_2 on a microscopic scale, 2) preferred *c*-orientation of the membrane, which results in significant reduction in grain boundary defect density on a mesoscopic scale, and 3) ultrathin thickness, which leads to reduced diffusion path length and therefore, higher H_2 permeance. In addition, both H_2/N_2 and H_2/CH_4 selectivity of *c*-oriented ultrathin MIL-96 membrane was superior to *a*-&*b*-oriented counterpart. The reason why the permeances of N_2 and CH_4 were higher than CO_2 could be attributed to preferential adsorption of CO_2 in MIL-96 framework than N_2 and CH_4 as evidenced by adsorption isotherms of CO_2, N_2 and CH_4 on MIL-96 powders (shown in Fig. S7), resulting in retarded diffusion of CO_2 through the MIL-96 membrane. It was further noticed that both H_2 permeance and SF of equimolar H_2/CO_2 gas mixture was constant within 24 h under ambient

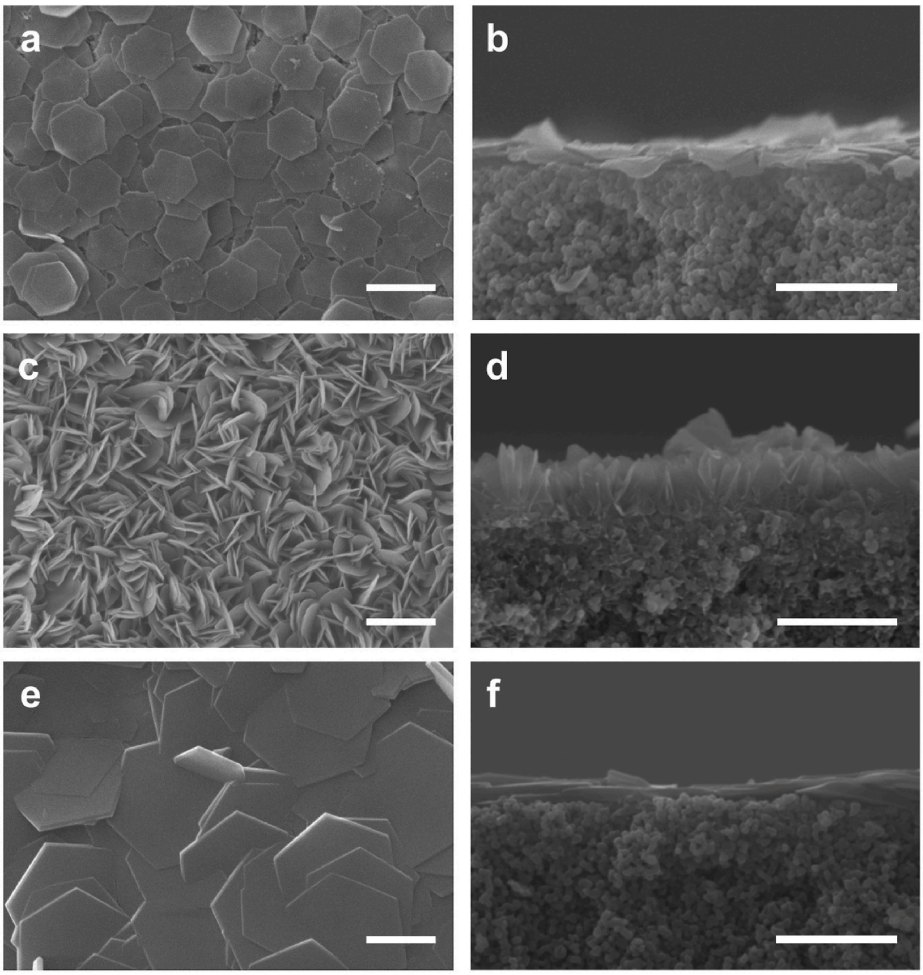

Fig. 4. SEM images of (a, b) *c*-oriented MIL-96 seed layer; (c, d) *a*-&*b*-oriented MIL-96 membrane; and (e, f) highly *c*-oriented ultrathin MIL-96 membrane. Scale bar: 2 μm.

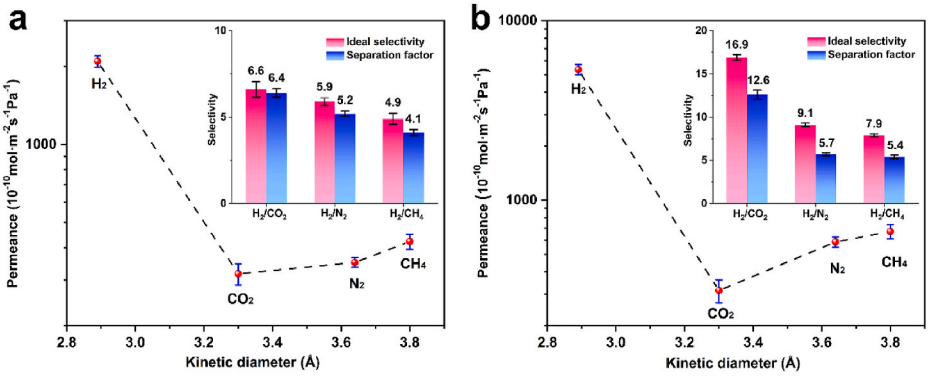

Fig. 5. Single-gas and equimolar binary gas mixture permeation results of a) *a*-&*b*-oriented MIL-96 membrane and b) *c*-oriented MIL-96 membrane under ambient conditions.

conditions (shown in Fig. S8) and elevated pressure (shown in Fig. S9), implying that prepared MIL-96 membrane possessed excellent long-term stability, which was indispensable for practical application in chemical industry.

4. Conclusions

To summarize, in this study we pioneered to prepare highly *c*-oriented ultrathin MIL-96 membrane by oriented seeded growth. Among various synthetic parameters, the preparation of ultrathin MIL-96 NS seeds through solvent optimization, the addition of trace amount of PVP in the seed suspension for spin coating, and the use of NMF as solvent during secondary growth were found to be crucial for obtaining the MIL-96 membrane with desired microstructure. Since the pore size of MIL-96 crystal structure along the *c*-axis was the smallest, prepared *c*-oriented ultrathin MIL-96 membrane exhibited better H_2/CO_2, H_2/N_2 and H_2/CH_4 selectivity compared with that of *a*-&*b*-orientation counterpart. Our research highlighted the importance of solvent composition

optimization in obtaining high-aspect-ratio MIL-96 NS seeds and relevant *c*-oriented ultrathin membrane as well as the significance of concurrent orientation and thickness control in separation performance enhancement of MOF membranes.

Author statement

Prof. Yi Liu conceived the idea and designed the experiments. Sixing Chen performed major experiments and analyzed the experimental data. Yi Liu helped with the characterization of MIL-96 NSs. Yanwei Sun drew the crystal structure of MIL-96 with the Mercury software. Guoliang Xu helped with the synthesis of MIL-96 NSs. Taotao Ji helped with relevant morphological characterization. Xiongfu Zhang assisted in analyzing the experimental data. Fei Wang helped with the pore size synthesis of MIL-96. Prof. Yi Liu and Sixing Chen co-wrote the manuscript with contributions from all authors. We all authors guarantee that the above information is reliable and correct.

Declaration of competing interest

The authors declare that they have no known competing financial interests or personal relationships that could have appeared to influence the work reported in this paper.

Acknowledgements

The authors are grateful to National Natural Science Foundation of China (22078039, 21176231), Fok Ying Tong Education Foundation of China (171063), Science and Technology Innovation Fund of Dalian (2020JJ26GX026), Science Fund for Creative Research Groups of the National Natural Science Foundation of China (22021005), the National Key Research and Development Program of China (2019YFE0119200), and the Technology Innovation Team of Dalian University of Technology (DUT2017TB01) for the financial support.

Appendix A. Supplementary data

Supplementary data to this article can be found online at https://doi.org/10.1016/j.memsci.2021.120064.

References

[1] C. Zhang, B.-H. Wu, M.-Q. Ma, Z. Wang, Z.-K. Xu, Ultrathin metal/covalent-organic framework membranes towards ultimate separation, Chem. Soc. Rev. 48 (2019) 3811–3841, https://doi.org/10.1039/C9CS00322C.

[2] K. Yang, Y. Ban, A. Guo, M. Zhao, Y. Zhou, N. Cao, W. Yang, In-situ interfacial assembly of ultra-H_2-permeable metal-organic framework membranes for H_2/CO_2 separation, J. Membr. Sci. 611 (2020), https://doi.org/10.1016/j.memsci.2020.118419.

[3] Y. Song, Y. Sun, D. Du, M. Zhang, Y. Liu, L. Liu, T. Ji, G. He, Fabrication of c-oriented ultrathin TCPP-derived 2D MOF membrane for precise molecular sieving, J. Membr. Sci. 634 (2021), https://doi.org/10.1016/j.memsci.2021.119393.

[4] Y. Li, H. Liu, H. Wang, J. Qiu, X. Zhang, GO-guided direct growth of highly oriented metal organic framework nanosheet membranes for H_2/CO_2 separation, Chem. Sci. 9 (2018) 4132–4141, https://doi.org/10.1039/c7sc04815g.

[5] P. Nian, H. Liu, X. Zhang, Bottom-up fabrication of two-dimensional Co-based zeolitic imidazolate framework tubular membranes consisting of nanosheets by vapor phase transformation of Co-based gel for H_2/CO_2 separation, J. Membr. Sci. 573 (2019) 200–209, https://doi.org/10.1016/j.memsci.2018.11.076.

[6] M. Tian, F. Pei, M. Yao, Z. Fu, L. Lin, G. Wu, G. Xu, H. Kitagawa, X. Fang, Ultrathin MOF nanosheet assembled highly oriented microporous membrane as an interlayer for lithium-sulfur batteries, Energy Storage Mater 21 (2019) 14–21, https://doi.org/10.1016/j.ensm.2018.12.016.

[7] F. Yang, M. Wu, Y. Wang, S. Ashtiani, H. Jiang, A GO-induced assembly strategy to repair MOF nanosheet-based membrane for efficient H_2/CO_2 separation, ACS Appl. Mater. Interfaces 11 (2019) 990–997, https://doi.org/10.1021/acsami.8b19480.

[8] S. Wang, J. Liu, B. Pulido, Y. Li, D. Mahalingam, S.P. Nunes, Oriented zeolitic imidazolate framework (ZIF) nanocrystal films for molecular separation membranes, ACS Appl. Nano Mater. 3 (2020) 3839–3846, https://doi.org/10.1021/acsanm.0c00570.

[9] Y. Ying, Z. Yang, D. Shi, S.B. Peh, Y. Wang, X. Yu, H. Yang, K. Chai, D. Zhao, Ultrathin covalent organic framework film as membrane gutter layer for high-permeance CO_2 capture, J. Membr. Sci. 632 (2021), https://doi.org/10.1016/j.memsci.2021.119384.

[10] Y. Yoo, Z. Lai, H.-K. Jeong, Fabrication of MOF-5 membranes using microwave-induced rapid seeding and solvothermal secondary growth, Microporous Mesoporous Mater. 123 (2009) 100–106, https://doi.org/10.1016/j.micromeso.2009.03.036.

[11] Y.-S. Li, H. Bux, A. Feldhoff, G.-L. Li, W.-S. Yang, J. Caro, Controllable synthesis of metal-organic frameworks: from MOF nanorods to oriented MOF membranes, Adv. Mater. 22 (2010) 3322–3326, https://doi.org/10.1002/adma.201000857.

[12] H. Bux, A. Feldhoff, J. Cravillon, M. Wiebcke, Y.-S. Li, J. Caro, Oriented zeolitic imidazolate framework-8 membrane with sharp H_2/C_3H_8 molecular sieve separation, Chem. Mater. 23 (2011) 2262–2269, https://doi.org/10.1021/cm200555s.

[13] X. Ma, Z. Wan, Y. Li, X. He, J. Caro, A. Huang, Anisotropic gas separation in oriented ZIF-95 membranes prepared by vapor-assisted in-plane epitaxial growth, Angew. Chem. Int. Ed. 59 (2020) 20858–20862, https://doi.org/10.1002/anie.202008260.

[14] Y. Sun, Y. Liu, J. Caro, X. Guo, C. Song, Y. Liu, In-plane epitaxial growth of highly c-oriented NH_2-MIL-125(Ti) membranes with superior H_2/CO_2 selectivity, Angew. Chem. Int. Ed. 57 (2018) 16088–16093, https://doi.org/10.1002/anie.201810088.

[15] Y. Sun, C. Song, X. Guo, Y. Liu, Concurrent manipulation of out-of-plane and regional in-plane orientations of NH_2-UiO-66 membranes with significantly reduced anisotropic grain boundary and superior H_2/CO_2 separation performance, ACS Appl. Mater. Interfaces 12 (2020) 4494–4500, https://doi.org/10.1021/acsami.9b18804.

[16] Y. Liu, Z. Ng, E.A. Khan, H.-K. Jeong, C.-B. Ching, Z. Lai, Synthesis of continuous MOF-5 membranes on porous alpha-alumina substrates, Microporous Mesoporous Mater. 118 (2009) 296–301, https://doi.org/10.1016/j.micromeso.2008.08.054.

[17] D. Zacher, O. Shekhah, C. Woell, R.A. Fischer, Thin films of metal-organic frameworks, Chem. Soc. Rev. 38 (2009) 1418–1429, https://doi.org/10.1039/b805038b.

[18] R. Ameloot, F. Vermoortele, W. Vanhove, M.B.J. Roeffaers, B.F. Sels, D.E. De Vos, Interfacial synthesis of hollow metal-organic framework capsules demonstrating selective permeability, Nat. Chem. 3 (2011) 382–387, https://doi.org/10.1038/nchem.1026.

[19] Y. Sun, F. Yang, Q. Wei, N. Wang, X. Qin, S. Zhang, B. Wang, Z. Nie, S. Ji, H. Yan, J.-R. Li, Oriented nano-microstructure-assisted controllable fabrication of metal-organic framework membranes on nickel foam, Adv. Mater. 28 (2016) 2374–2381, https://doi.org/10.1002/adma.201505437.

[20] J.-L. Zhuang, A. Terfort, C. Woell, Formation of oriented and patterned films of metal-organic frameworks by liquid phase epitaxy: a review, Coord. Chem. Rev. 307 (2016) 391–424, https://doi.org/10.1016/j.ccr.2015.09.013.

[21] Z. Kang, L. Fan, D. Sun, Recent advances and challenges of metal-organic framework membranes for gas separation, J. Mater. Chem. 5 (2017) 10073–10091, https://doi.org/10.1039/c7ta01142c.

[22] H. Zhu, D. Liu, The synthetic strategies of metal-organic framework membranes, films and 2D MOFs and their applications in devices, J. Mater. Chem. 7 (2019) 21004–21035, https://doi.org/10.1039/c9ta05383b.

[23] T. Loiseau, L. Lecroq, C. Volkringer, J. Marrot, G. Ferey, M. Haouas, F. Taulelle, S. Bourrelly, P.L. Llewellyn, M. Latroche, MIL-96, A porous aluminum trimesate 3D structure constructed from a hexagonal network of 18-membered rings and mu(3)-oxo-centered trinuclear units, J. Am. Chem. Soc. 128 (2006) 10223–10230, https://doi.org/10.1021/ja0621086.

[24] M. Haouas, C. Volkringer, T. Loiseau, G. Ferey, F. Taulelle, In situ NMR, ex situ XRD and SEM study of the hydrothermal crystallization of nanoporous aluminum trimesates MIL-96, MIL-100, and MIL-110, Chem. Mater. 24 (2012) 2462–2471, https://doi.org/10.1021/cm300439e.

[25] C. Volkringer, T. Loiseau, G. Ferey, C.M. Morais, F. Taulelle, V. Montouillout, D. Massiot, Synthesis, crystal structure and Ga-71 solid state NMR of a MOF-type gallium trimesate (MIL-96) with mu(3)-oxo bridged trinuclear units and a hexagonal 18-ring network, Microporous Mesoporous Mater. 105 (2007) 111–117, https://doi.org/10.1016/j.micromeso.2007.05.018.

[26] C. Volkringer, D. Popov, T. Loiseau, G. Ferey, M. Burghammer, C. Riekel, M. Haouas, F. Taulclle, Synthesis, single-crystal X-ray microdiffraction, and NMR characterizations of the giant pore metal-organic framework aluminum trimesate MIL-100, Chem. Mater. 21 (2009) 5695–5697, https://doi.org/10.1021/cm901983a.

[27] M. Gaab, N. Trukhan, S. Maurer, R. Gummaraju, U. Mueller, The progression of Al-based metal-organic frameworks - from academic research to industrial production and applications, Microporous Mesoporous Mater. 157 (2012) 131–136, https://doi.org/10.1016/j.micromeso.2011.08.016.

[28] M. Benzaqui, R.S. Pillai, A. Sabetghadam, V. Benoit, P. Normand, J. Marrot, N. Menguy, D. Montero, W. Shepard, A. Tissot, C. Martineau-Corcos, C. Sicard, M. Mihaylov, F. Carn, I. Beurroies, P.L. Llewellyn, G. De Weireld, K. Hadjiivanov, J. Gascon, F. Kapteijn, G. Maurin, N. Steunou, C. Serre, Revisiting the aluminum trimesate-based MOF (MIL-96): from structure determination to the processing of mixed matrix membranes for CO_2 capture, Chem. Mater. 29 (2017) 10326–10338, https://doi.org/10.1021/acs.chemmater.7b03203.

[29] L. Wen, J. Su, X. Wu, P. Cai, W. Luo, G. Cheng, Ruthenium supported on MIL-96: an efficient catalyst for hydrolytic dehydrogenation of ammonia borane for chemical hydrogen storage, Int. J. Hydrogen Energy 39 (2014) 17129–17135, https://doi.org/10.1016/j.ijhydene.2014.07.179.

[30] M.A. Andres, M.T. Vijjapu, S.G. Surya, O. Shekhah, K.N. Salama, C. Serre, M. Eddaoudi, O. Roubeau, I. Gascon, Methanol and humidity capacitive sensors based on thin films of MOF nanoparticles, ACS Appl. Mater. Interfaces 12 (2020) 4155–4162, https://doi.org/10.1021/acsami.9b20763.

[31] V. Benoit, N. Chanut, R.S. Pillai, M. Benzaqui, I. Beurroies, S. Devautour-Vinot, C. Serre, N. Steunou, G. Maurin, P.L. Llewellyn, A promising metal-organic framework (MOF), MIL-96(Al), for CO_2 separation under humid conditions, J. Mater. Chem. 6 (2018) 2081–2090, https://doi.org/10.1039/c7ta09696h.
[32] X. Wang, H. Zhu, T. Sun, Y. Liu, T. Han, J. Lu, H. Dai, L. Zhai, Synthesis and study of an efficient metal-organic framework adsorbent (MIL-96(Al)) for fluoride removal from water, J. Nanomater. 2019 (2019) 3128179, https://doi.org/10.1155/2019/3128179.
[33] J. Li, M.J. Hurlock, V.G. Goncharov, X. Li, X. Guo, Q. Zhang, Solvent-free and phase-selective synthesis of aluminum trimesate metal-organic frameworks, Inorg. Chem. 60 (2021) 4623–4632, https://doi.org/10.1021/acs.inorgchem.0c03598.
[34] A. Knebel, S. Friebe, N.C. Bigall, M. Benzaqui, C. Serre, J. Caro, Comparative study of MIL-96(Al) as continuous metal-organic frameworks layer and mixed-matrix membrane, ACS Appl. Mater. Interfaces 8 (2016) 7536–7544, https://doi.org/10.1021/acsami.5b12541.
[35] D. Liu, Y. Liu, F. Dai, J. Zhao, K. Yang, C. Liu, Size- and morphology-controllable synthesis of MIL-96 (Al) by hydrolysis and coordination modulation of dual aluminium source and ligand systems, Dalton Trans. 44 (2015) 16421–16429, https://doi.org/10.1039/c5dt02379c.
[36] B. Seoane, A. Dikhtiarenko, A. Mayoral, C. Tellez, J. Coronas, F. Kapteijn, J. Gascon, Metal organic framework synthesis in the presence of surfactants: towards hierarchical MOFs, CrystEngComm 17 (2015) 1693–1700, https://doi.org/10.1039/c4ce02324b.
[37] C. Gu, J. Li, G. Yang, L. Zhang, C.-S. Liu, H. Pang, Morphology and size-controlled synthesis of Co-doped MIL-96 by different alkaline modulators for sensitively detecting alpha-fetoprotein, Chin. Chem. Lett. 31 (2020) 2263–2267, https://doi.org/10.1016/j.cclet.2020.02.044.
[38] L.H.M. Azmi, D.R. Williams, B.P. Ladewig, Polymer-assisted modification of metal-organic framework MIL-96 (Al): influence of HPAM concentration on particle size, crystal morphology and removal of harmful environmental pollutant PFOA, Chemosphere 262 (2021) 128072, https://doi.org/10.1016/j.chemosphere.2020.128072.
[39] C. O'Connor, Acidic and basic amide hydrolysis, Q. Rev. Chem. Soc. 24 (1970) 553–564, https://doi.org/10.1039/QR9702400553.
[40] J. Zhou, W. Cai, Z. Yang, Q. Xia, J. Chen, J. Fan, C. Du, N,N-dimethylformamide assisted facile hydrothermal synthesis of boehmite microspheres for highly effective removal of Congo red from water, J. Colloid Interface Sci. 583 (2021) 128–138, https://doi.org/10.1016/j.jcis.2020.09.004.
[41] Q. Qian, P.A. Asinger, M.J. Lee, G. Han, K.M. Rodriguez, S. Lin, F.M. Benedetti, A. X. Wu, W.S. Chi, Z.P. Smith, MOF-based membranes for gas separations, Chem. Rev. 120 (2020) 8161–8266, https://doi.org/10.1021/acs.chemrev.0c00119.
[42] A. Vander Drift, Evolutionary selection A principle governing growth orientation in vapour-deposited layers, Philips Res. Rep. 22 (1967) 267–288.